



# Development of the microstructure and crystallographic texture during annealing of a rolled polycrystalline Fe<sub>3</sub>Al alloy

D. Raabe, J. Keichel

*Institut für Metallkunde und Metallphysik, Kopernikusstrasse 14, RWTH Aachen, 52056 Aachen, Germany*

Received 21 March 1995; in revised form 5 May 1995

## Abstract

The evolution of the microstructure and crystallographic texture of a polycrystalline Fe<sub>3</sub>Al alloy during rolling and subsequent annealing was studied. For this purpose optical microscopy, single orientation determination in the scanning electron microscope and X-ray texture measurements were carried out on both rolled and annealed specimens. During warm rolling ( $\epsilon_{\max} = 80\%$ ,  $T_{\text{roll}} = 560$  °C) a strong texture fibre close to  $\{111\}\langle uvw \rangle$  with a maximum at  $\{557\}\langle 110 \rangle$  was developed. During the subsequent heat treatment (750 °C, salt bath) the orientation distribution did not change substantially, i.e. the texture close to  $\{111\}\langle uvw \rangle$  was essentially preserved. For annealing times less than 50 s the  $\{557\}\langle 110 \rangle$  orientation remained the dominant texture component. For annealing times exceeding 50 s the  $\{557\}\langle 110 \rangle$  orientation considerably decreased and the  $\{111\}\langle 112 \rangle$  orientation, which was nearly unaffected by annealing, became the main orientation. These texture changes, which were studied in detail by use of single orientation determination, were interpreted in terms of preferred recovery in  $\{111\}\langle 112 \rangle$  and preferred recrystallization in  $\{557\}\langle 110 \rangle$  oriented grains.

*Keywords:* Fe<sub>3</sub>Al; Texture; Microstructure; Recrystallization; Recovery

## 1. Introduction

Intermetallic iron aluminides with compositions near that of FeAl ordered to the B2 structure and Fe<sub>3</sub>Al ordered to the B2 or DO<sub>3</sub> structure have long been studied owing to their good mechanical properties and excellent oxidation and sulphidation resistance [1–7]. Among these aluminides imperfectly B2 ordered Fe<sub>3</sub>Al-based alloys containing ternary additions in substitutional solution (Cr, Mo, Zr, Nb, Hf) and further additions in interstitial solution (C, B) have increasingly attracted attention in industrial terms [7–11]. Due to the control of composition, structure and microstructure, both the mechanical properties and the corrosion resistance of such complex alloys were considerably improved, especially the room temperature ductility and the strength at elevated temperatures [8–12]. Most alloys presently under investigation reveal a B2 type structure with imperfect long-range order. Pure iron aluminides with more than 24 at.% aluminium content typically reveal a DO<sub>3</sub> long-range order after slow

cooling of only 10–20 K per day [7,13–16]. However, in the cases of rapid cooling or thermomechanical treatment of complex Fe<sub>3</sub>Al-based alloys, extensive primary solid solutions have been observed which include long-range ordered areas based upon both the B2 and DO<sub>3</sub> structures [4,7,10,11].

Recent studies focused on the investigation of the mechanisms of plastic deformation of such imperfectly ordered iron aluminides. In this context three methods were chiefly employed. First, the slip traces on polished specimen surfaces were analysed [17,18]. Second, slip planes and Burgers vectors of dislocations were examined via transmission electron microscopy (TEM) [19–22]. Third, the influence of the antiphase boundary energy was estimated on the selection of the glide systems [23,24]. In most investigations it was observed that dislocations in perfectly or imperfectly B2 and DO<sub>3</sub> ordered iron aluminides move at elevated temperatures on such slip systems, which are usually activated in non-ordered body centred cubic (b.c.c.) alloys. Whereas the occurrence of  $\{110\}\langle 111 \rangle$  slip systems seemed to be

promoted by the low antiphase boundary energy, the strong tendency for  $\{112\}\langle 111\rangle$  slip, especially at low temperatures was interpreted in terms of dislocation core effects [25]. Additionally, the activation of glide systems with a  $\langle 100\rangle$  Burgers vector and  $\{001\}$  or  $\{110\}$  slip planes was predicted [26]. Thorough reviews on this subject were published by Umakoshi [27] and McKamey et al. [7].

Whereas the fundamentals of plastic deformation of iron aluminides were the subject of various thorough studies the underlying mechanisms of recovery and recrystallization have not yet been tackled accordingly in the literature. As was recently discussed by Morris et al. [12,28], the properties of  $\text{Fe}_3\text{Al}$  alloys are essentially determined by the final annealing treatment of heavily warm rolled samples ( $\epsilon = 80\text{--}85\%$ ). In their investigation [12] they observed that at annealing temperatures within the range  $600\text{--}800\text{ }^\circ\text{C}$  recovery prevailed, and at  $850\text{ }^\circ\text{C}$  primary recrystallization prevailed. One of the main results of their study was that both the strength and the ductility of recovered specimens considerably exceeded the values obtained for primary recrystallized specimens. This was attributed to the formation of  $\langle 100\rangle$  dislocation networks during recovery, which were suggested to act as barriers to further dislocation motion. However, the best ductility was not obtained for samples annealed at  $600\text{ }^\circ\text{C}$  but for those annealed at  $700\text{ }^\circ\text{C}$ . Such a result is surprising if one entirely attributes the enhancement of ductility to the recovery process. Since the activation energy of primary recrystallization typically exceeds that of recovery one should expect the best ductility for samples which were annealed at low temperatures. Furthermore, it is well known from investigations on non-ordered b.c.c. metals and alloys that the recrystallization behaviour considerably depends on the individual grain orientation. In b.c.c. metals it was frequently observed that the reformation of the grain morphology upon annealing took place in a heterogeneous manner, leading to both recovery and recrystallization depending on the orientation of the crystal affected [29–31].

The present study hence concentrates on the investigation of the development of the crystallographic texture and microstructure during annealing of heavily warm rolled  $\text{Fe}_3\text{Al}$  polycrystals for the following reasons.

1. During recrystallization newly formed large-angle boundaries have the kinematic freedom to sweep as incoherent interfaces freely through the deformed matrix. The generation of these boundaries requires an incubation period. In contrast, recovery does not require an incubation period. Non-conservative dislocation rearrangement and dislocation annihilation, which reduce internal stresses, continuously seize the entire specimen from the beginning of heat treatment. Due to the mechanisms involved, recrystallization discontinuously changes the texture while recovery preserves the texture. It is hence obvious that the investigation of orientation changes is an appropriate diagnostic means of distinguishing between both mechanisms. In the present study texture changes were examined both statistically (X-ray diffraction,  $\sim 10^4$  grains, no spatial resolution) and locally (electron backscattering diffraction, single grains, spatial resolution).

2. In technical terms the directional behaviour of polycrystalline material is generally an integral property of its orientation distribution.  $\text{Fe}_3\text{Al}$ -based alloys are considered as potential candidates for applications where ferritic stainless steels with an elevated Cr content are presently in use [7–11]. For this reason their directional plastic properties, especially their deep drawing behaviour after the final heat treatment, should be studied. The first investigations of the crystallographic textures of deformed and heat-treated polycrystalline iron aluminides and comparable B2 ordered alloys have been recently published by Mao and Sun [32,33] and Raabe [34–36].

## 2. Experimental

### 2.1. Sample preparation

An  $\text{Fe}_3\text{Al}$  alloy with 15.7% Al, 0.088% Cr,  $< 0.05\%$  Zr, 0.02% Mo and 0.06% C (% = mass%) was cast, thermomechanically hot rolled and finally annealed at  $600\text{ }^\circ\text{C}$  [10,11]. In this state the grain size was about  $200\text{ }\mu\text{m}$ . The latter two manufacturing steps are referred to as B2 treatment [10,11]. Subsequently, the sheet was warm rolled at  $530\text{--}560\text{ }^\circ\text{C}$  to  $\epsilon = 80\%$ . The final sheet had an imperfectly ordered B2 structure [10,11]. Dynamic recrystallization was not observed during warm rolling. Subsequently, the specimens were annealed in a salt bath furnace at a temperature of  $750\text{ }^\circ\text{C}$  for 1–5000 s. The microstructure of the rolled and annealed samples was studied by means of optical and electron microscopy. For this purpose the specimens were etched in pure HCl for 1–3 min or in a solution of 10 ml  $\text{H}_2\text{O}_2$  and 1 ml HF for about 30 s.

### 2.2. Measurement and presentation of crystallographic textures

The crystal textures of the warm rolled and finally annealed specimens were examined using both statistical and local orientation determination. In the first case the experiments were carried out using an X-ray texture goniometer equipped with  $\text{MoK}\alpha$  radiation. The four pole figures  $\{220\}$ ,  $\{400\}$ ,  $\{422\}$  and  $\{620\}$  were measured in the back reflection mode. From the two-di-

dimensional, centrosymmetric pole figures the quantitative three-dimensional orientation distribution function (ODF) was computed using the iterative harmonic method ( $l_{\max} = 22$ ) [37,38]. Using this technique provided orientation data stemming from about  $10^4$  grains, but no spatial resolution. In the second case the texture was examined at the grain scale, exploiting the orientation dependence of electron backscattering diffraction (EBSD) [39]. This technique represents a useful means of providing both microstructure and texture data with a high spatial resolution. Details of the latter technique have been explained elsewhere [40]. All texture measurements were carried out in the centre layer of the specimens. For this purpose the samples were ground and finally etched by use of pure HCl.

In the case of cubic crystal symmetry and orthorhombic sample symmetry an orientation can be presented by using the three Euler angles  $\varphi_1$ ,  $\phi$ ,  $\varphi_2$  or the Miller Indices  $\{hkl\}\langle uvw \rangle$ , where the first triple indicates the crystallographic plane parallel to the sheet surface and the second one the crystal vector parallel to the rolling direction. Relevant texture components which are typically generated during rolling and annealing of B2 type aggregates [32–36] are positioned on the so called  $\alpha$ -fibre,  $\{hkl\}\langle 110 \rangle$ , and  $\gamma$ -fibre,  $\{111\}\langle uvw \rangle$ . The first orientation tube at  $\varphi_1 = 0^\circ$  and  $\varphi_2 = 45^\circ$  comprises all texture components with a crystallographic  $\langle 110 \rangle$  direction parallel to the rolling direction, e.g.  $\{001\}\langle 110 \rangle$  at  $\phi = 0^\circ$ ,  $\{112\}\langle 110 \rangle$  at  $\phi \sim 35^\circ$  and  $\{111\}\langle 110 \rangle$  at  $\phi = 54.7^\circ$ . The second fibre at  $\phi = 54.7^\circ$  and  $\varphi_2 = 45^\circ$  includes all texture components with a crystallographic  $\langle 111 \rangle$  direction parallel to the normal

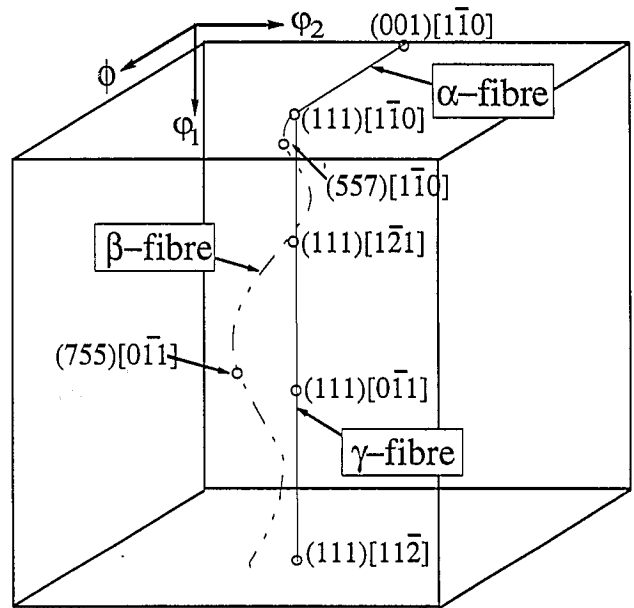


Fig. 1. Reduced Euler space ( $0 \leq \varphi_1 \leq \pi/2$ ,  $0 \leq \phi \leq \pi/2$ ,  $0 < \varphi_2 \leq \pi/2$ ) with some important texture components typically observed in rolled B2 and DO<sub>3</sub> ordered iron aluminides [32–36].

direction of the sheet, e.g.  $\{111\}\langle 110 \rangle$  at  $\varphi_1 = 0^\circ$ ,  $60^\circ$  and  $\{111\}\langle 112 \rangle$  at  $\varphi_1 = 30^\circ$ ,  $90^\circ$ . Since often some texture components are not exactly positioned on the  $\gamma$ -fibre, the  $\beta$ -fibre sometimes provides a more appropriate description of the texture. This fibre does not follow fixed coordinates in Euler space but changes its course according to the maximum orientation densities in the vicinity ( $\pm 15^\circ$ ) of the  $\gamma$ -fibre (Fig. 1). The single orientation data are presented by use of  $\{200\}$  pole figures.

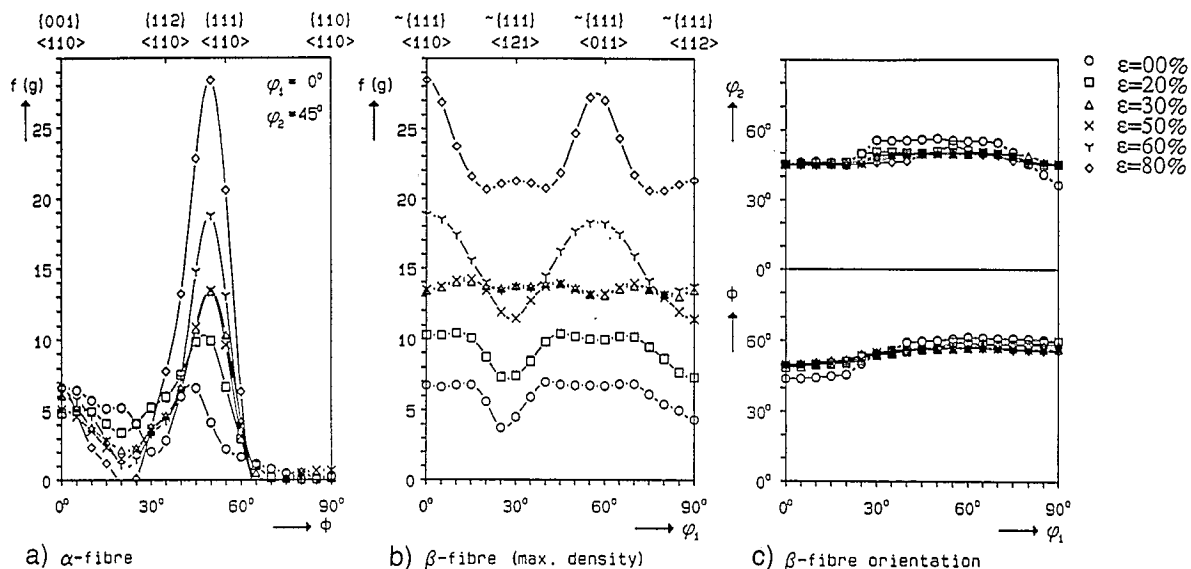


Fig. 2. Warm rolling texture ( $T = 530\text{--}560^\circ\text{C}$ ) after  $\epsilon = 0\%$ ,  $20\%$ ,  $30\%$ ,  $50\%$ ,  $60\%$  and  $80\%$  as determined in the centre layer of the specimens; orientation distribution function calculated by use of the iterative series expansion method ( $l_{\max} = 22$ ) [37,38]. (a)  $\alpha$ -fibre; (b)  $\beta$ -fibre, orientation density; (c)  $\beta$ -fibre, coordinates in Euler space.

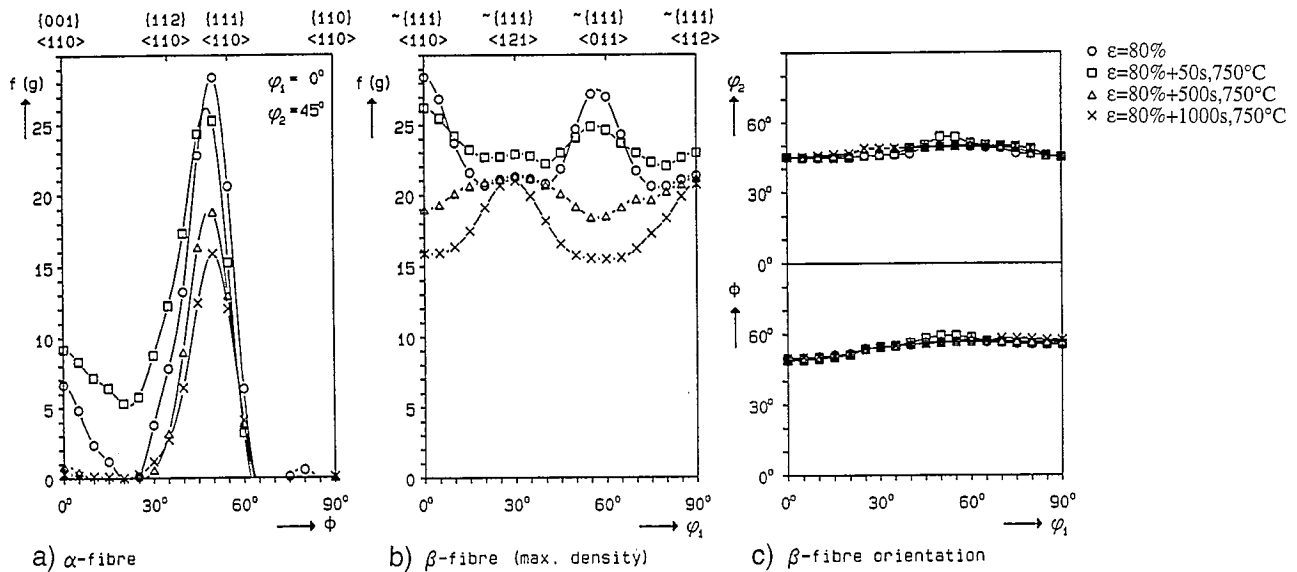


Fig. 3. Annealing texture of the 80% warm rolled and subsequently heat treated specimen after 50 s, 500 s and 1000 s at 750 °C in a salt bath furnace. (a)  $\alpha$ -fibre; (b)  $\beta$ -fibre, orientation density; (c)  $\beta$ -fibre, coordinates in Euler space.

### 3. Results

#### 3.1. Rolling textures

Fig. 2 shows the starting texture, i.e. the orientation distribution after casting, thermomechanical hot rolling and hot band annealing ( $\epsilon = 0\%$ ) and the warm rolling textures after  $\epsilon = 20\%$ ,  $30\%$ ,  $50\%$ ,  $60\%$  and  $80\%$  as determined in the centre layer of the specimens. The starting texture ( $\epsilon = 0\%$ ) is characterized by a weak  $\alpha$ -fibre (Fig. 2(a)) and a weak  $\beta$ -fibre (Fig. 2(b)). The maximum occurring orientation density is quite small,  $f(g)_{\max} = 6.8$ . In the microstructure of the starting sample mainly equiaxed or slightly elongated grains were found, which means that recrystallization has taken place during or subsequent to the thermomechanical treatment. After 20%, 30% and 50% rolling deformation the texture reveals a main component  $\{557\}\langle 110 \rangle$  which is close to  $\{111\}\langle 110 \rangle$  and a weak  $\{001\}\langle 110 \rangle$  orientation on the  $\alpha$ -fibre (Fig. 2(a)). The  $\beta$ -fibre (Fig. 2(b)) shows again the dominant  $\{557\}\langle 110 \rangle$  and the somewhat weaker  $\{111\}\langle 112 \rangle$  orientation. Fig. 2(c) shows the  $\beta$ -fibre coordinates for both orientations. Whereas the  $\{111\}\langle 112 \rangle$  component is exactly located on the  $\gamma$ -fibre, the  $\{557\}\langle 110 \rangle$  orientation is less symmetric, as indicated by its Miller indices. As has been shown in previous papers, this type of rolling texture, especially the absence of the  $\{112\}\langle 110 \rangle$  component, is typical of rolling textures of B2 ordered alloys [32–36]. After large degrees of warm rolling,  $\epsilon = 60\%$  and  $\epsilon = 80\%$ , the  $\beta$ -fibre gradually increases. The maximum texture component is positioned at  $\{557\}\langle 110 \rangle$  (Figs. 2(a), (b)).

#### 3.2. Annealing textures and microstructure

Fig. 3 shows the  $\alpha$ - and the  $\beta$ -fibre of the 80% warm rolled and annealed specimen after 50 s, 500 s and 1000 s at 750 °C. The texture maximum at  $\{557\}\langle 110 \rangle$  continuously decreases with the increase of the annealing time (Figs. 3(a), (b)). The weak initial  $\{001\}\langle 110 \rangle$  orientation is slightly sharpened after 50 s and finally decreased after longer annealing times (Fig. 3(a)). The  $\beta$ -fibre (Fig. 3(b)) not only shows the degradation of the  $\{557\}\langle 110 \rangle$  orientation but additionally reveals the maintenance of the  $\{111\}\langle 112 \rangle$  component. After 50 s even a slight increase of the  $\{111\}\langle 112 \rangle$  orientation ( $\phi_1 = 30^\circ, 90^\circ$ ) is revealed which balances the decrease of the  $\{557\}\langle 110 \rangle$  component ( $\phi_1 \sim 0^\circ, 60^\circ$ ) (Fig. 3(b)). As is evident from Fig. 3(c) the position of the  $\beta$ -fibre in Euler space is not affected by the anneal.

The longitudinal sections of the corresponding microstructure (Fig. 4) show a state of partial reformation of the microstructure by recrystallization or recovery after 50 s at 750 °C (Fig. 4(a)). After 500 s (Fig. 4(b)) and 1000 s (Fig. 4(c)) at 750 °C the deformation microstructure is nearly removed. However, from these micrographs it cannot be firmly decided whether recovery or recrystallization processes prevailed during annealing. Although numerous grain boundaries seem to possess large angles with respect to the surrounding deformation microstructure the hue of the grains in the micrographs does not necessarily represent a quantitative measure for their orientation.

In order to examine whether recovery or recrystallization prevailed during reformation of the microstructure of 80% rolled specimens at 750 °C the early stages of annealing (after 20 s) were studied in

grain scale using EBSD (Figs. 5 and 6). Three main results were obtained from these experiments:

1. Numerous newly formed areas were identified to arise from recovery rather than from recrystallization. These new grains were essentially characterized by two features. First, they typically revealed small angles of less than  $20^\circ$  with respect to the surrounding deformation microstructure. Second, they were often located within the deformed grains rather than at former large angle grain boundaries. However, it was observed that recovered areas were frequently accompanied by new grains with large angle grain boundaries. An example is shown in Fig. 5, where a number of newly formed areas can be seen, some of which revealed small and some large angle boundaries with respect to the neighbouring microstructure. The areas marked as D and C had misorientations within the range  $18\text{--}27^\circ$  with respect to the deformed host grain, B, which had an orientation  $\sim \{772\}\langle 027 \rangle$ . The misorientation between A and B was somewhat larger. In contrast to



Fig. 4. Longitudinal micrographs showing the warm rolled specimens after annealing at  $750^\circ\text{C}$  in a salt bath furnace. (a) 50 s, (b) 500 s, (c) 1000 s.

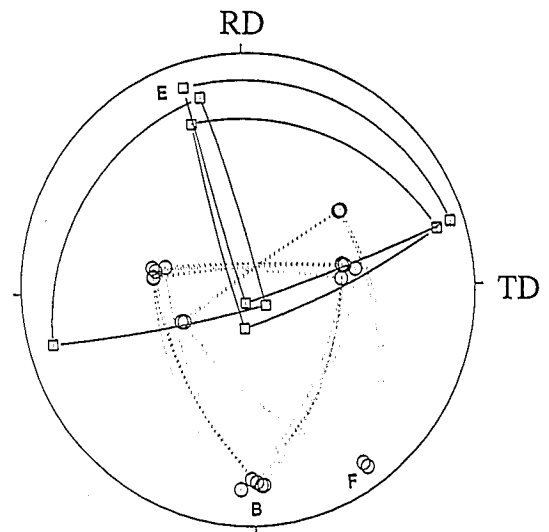
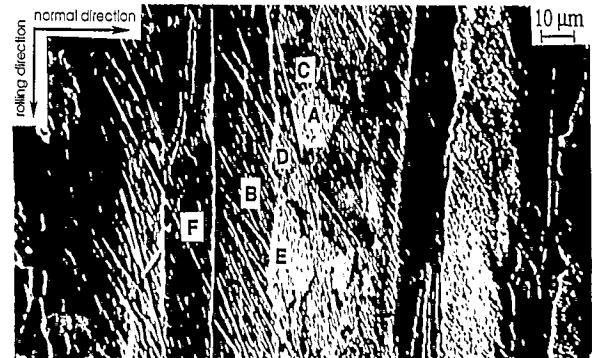
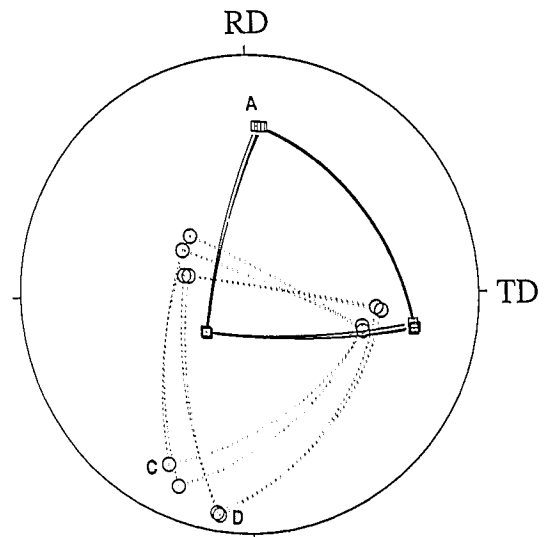


Fig. 5. Longitudinal micrograph showing various deformed and new grains at an early stage of the anneal (20 s,  $750^\circ\text{C}$ , salt bath). Some of the relevant orientations are given in  $\{200\}$  pole figures.

these orientation relationships, some of which were still within the range of small angle grain boundaries, the newly formed grain E showed a misorientation of  $42\text{--}48^\circ$  with respect to the deformed grain, B (Fig. 5).

2. A large number of isolated newly formed grains was observed on former high angle grain boundaries.

These grains typically revealed misorientations in excess of  $20^\circ$  with respect to the neighbouring deformation microstructure on at least either side. An example is shown in Fig. 6, where the orientations obtained from the newly formed grain, A, are marked by solid lines in the  $\{200\}$  pole figures. The grain orientations belonging to group B (Fig. 6) were split into two main texture components, viz.  $\{557\}\langle 377 \rangle$  in the direct vicinity of grain A and  $\sim\{538\}\langle 385 \rangle$  at a distance of about  $10\ \mu\text{m}$  from the new grain. The misorientation of the new grain with respect to the neighbouring  $\sim\{557\}\langle 377 \rangle$  oriented matrix amounted to about  $21^\circ$ . The misorientation between grain A and grain C, the orientation of which was close to  $\sim\{039\}\langle 862 \rangle$  even amounted to  $25^\circ$ . (The descriptions of the orientations here are approximate. Mathematically, the vectors  $hkl$  and  $uvw$  must be perpendicular.)

- For a large number of neighbouring deformed and recovered areas which were related by angles within the range  $15\text{--}25^\circ$  the rotation axis common to both

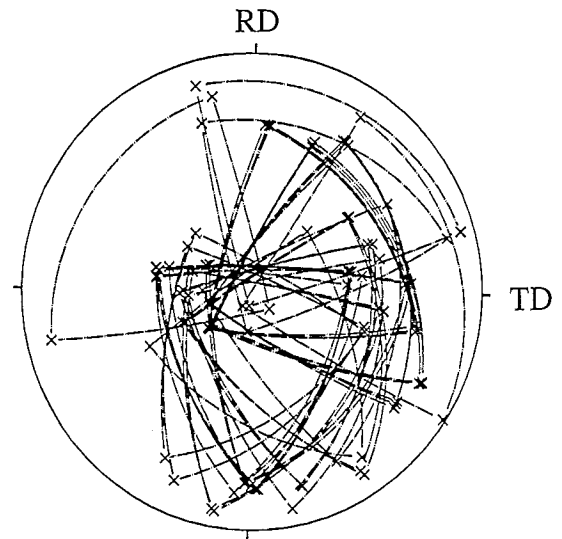


Fig. 7.  $\{200\}$  pole figure showing the orientations of various neighbouring recovered areas at an early stage of the anneal (20 s,  $750^\circ\text{C}$ , salt bath). It becomes apparent that some neighbouring areas reveal a common  $\langle 100 \rangle$  rotation axis.

regions was often very close to a  $\langle 100 \rangle$  vector. This is exemplary shown in Fig. 7 for a group of recovered regions which often revealed a common rotation axis close to  $\langle 100 \rangle$ .

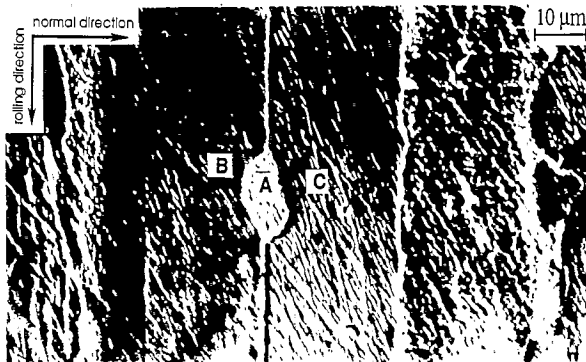
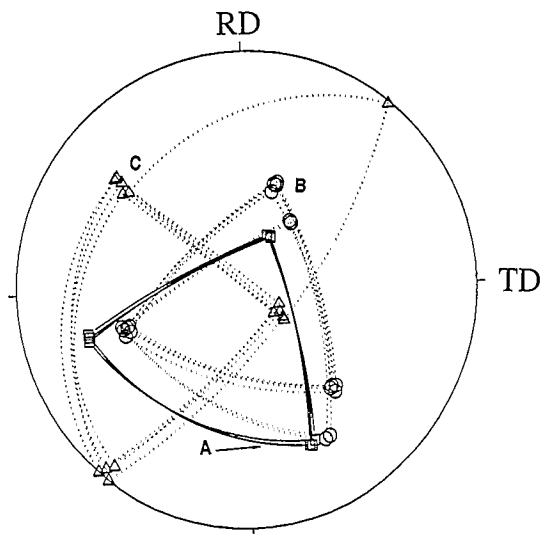


Fig. 6. Longitudinal micrograph showing various deformed grains and a single new grain which is located on a former large angle grain boundary at an early stage of the anneal (20 s,  $750^\circ\text{C}$ , salt bath). Some of the relevant orientations are given in the  $\{200\}$  pole figure.

## 4. Discussion

### 4.1. Rolling texture

The rolling textures of  $\text{Fe}_3\text{Al}$  (Fig. 3) can be interpreted in terms of Taylor type simulations [34–36,41], which are based on the description of macroscopic deformation by means of dislocation slip. Macroscopic deformation is characterized by the velocity gradient tensor written in lattice coordinates. Its symmetric part represents the strain rate tensor and the antisymmetric part describes the spin. From the latter tensor and the velocity gradient tensor written in machine coordinates the relevant lattice rotations can be computed. In the so called Full Constraints (FC) Taylor model [41] the imposed strain tensor is entirely transferred into each grain, where it is fulfilled by crystallographic slip. Incompatibilities between neighbouring grains are hence avoided. In the various variants of the so-called Relaxed Constraints (RC) Taylor type approach [42] some of the external shear components are not transferred into the grain, i.e. the occurrence of shear strains between neighbouring grains is conceded locally. Relaxing the strain component  $\epsilon_{13}$  corresponds to a shear in the longitudinal direction, while  $\epsilon_{23}$  denotes transverse shear (directions 1, 2 and 3 refer to the rolling, transverse and normal direction, respectively). The relaxation of both  $\epsilon_{13}$  and  $\epsilon_{23}$  is referred to as the pancake model. Allowing for these shears leads to changes in the

texture evolution when compared to the predictions of the FC theory. As discussed previously [34–36] a good description of experimentally determined Fe<sub>3</sub>Al warm rolling textures was achieved by simulations on the basis of the pancake model in which both {110}<111> and {112}<111> slip systems were taken into account with an identical critical resolved shear stress.

#### 4.2. Annealing texture and microstructure

The investigation of the annealing texture and microstructure ( $\epsilon = 80\%$ , 750 °C) substantiated that recovery as well as primary recrystallization contributed to the reformation of the deformation microstructure during the anneal. However, both the X-ray and the EBSD texture investigations confirmed that these processes were not distributed in a statistical manner throughout the annealed specimens. It was found that both recovery and recrystallization took place preferably in deformed host grains with orientations which seemed to be characteristic of either of these two processes.

As is evident from Fig. 4, at the beginning of the anneal (50 s) the development of the two main  $\beta$ -fibre orientations, {557}<110> and {111}<112>, behave inversely. The {557}<110> component drops from  $f(g) \sim 27.5$  to  $f(g)_{50s} \sim 24.5$ , while {111}<112> slightly increases from  $f(g) \sim 21.2$  to  $f(g)_{50s} \sim 23$ . With increasing annealing time this behaviour becomes even more pronounced. Whereas {557}<110> decreases with the annealing time to  $f(g)_{1000s} \sim 15.5$ , {111}<112> stabilizes at  $f(g)_{1000s} \sim 21$ . Considering the fact that both texture components are very similar their different behaviour appears quite surprising.

The movement of high angle grain boundaries during recrystallization includes discontinuous orientation changes. In contrast, pronounced recovery leads to the stabilization of texture. In this context the results shown in Fig. 4 suggest that the {557}<110> component reveals a larger tendency to recrystallize as compared to the {111}<112> component which remains nearly unchanged during annealing. At first sight a plausible explanation for the different behaviour of both texture components during annealing might be their different Taylor factor,  $M$ . This parameter describes the total amount of crystallographic slip,  $\sum_{s=1}^5 \Delta\gamma^s$ , which is required to accomplish plastic deformation within an externally imposed strain increment,  $\Delta\epsilon_{11}$ , i.e.

$$M = \frac{1}{\Delta\epsilon_{11}} \sum_{s=1}^5 \Delta\gamma^s \quad (1)$$

Under Full Constraints Taylor conditions usually five slip systems are required to obtain mutual compatibility of the grains. Following this definition the Taylor factor may be regarded as a rough measure for the elastically stored energy of the grain considered and hence

for its tendency to recrystallize. Under the assumption of dislocation slip on {110}<111> glide systems a value of  $M = 3.67$  (FC) and  $M = 3.67$  (RC, pancake) is predicted for {111}<112> oriented grains and  $M = 3.72$  (FC) and  $M = 3.02$  (RC, pancake) for {557}<110> oriented grains. Since in Section 4.1. it is mentioned that the texture predictions of the RC pancake model are in better accord with experiment the latter values should be more reliable. Although the difference in the Taylor factors of both texture components is not very large, this approach even suggests a slightly weaker instead of stronger recrystallization tendency for {557}<110> oriented grains. This result seems to contradict the observations discussed above. Moreover, it is widely accepted [17,18,21–27] that both {110}<111> and {112}<111> slip systems contribute to the plastic deformation of Fe<sub>3</sub>Al alloys. As pointed out by Umakochi [27] the occurrence of {110}<111> slip systems seems to be promoted by their low anti-phase boundary energy and the strong tendency for {112}<111> slip, especially at low temperatures, probably stems from dislocation core effects. Considering both types of slip system with an identical critical resolved shear stress leads to  $M = 3.56$  (FC) and  $M = 3.19$  (RC, pancake) for {111}<112> oriented grains and  $M = 3.52$  (FC) and  $M = 2.87$  (RC, pancake) for {557}<110> oriented grains. Even on this more realistic basis the Taylor factors obviously do not provide a sufficiently unequivocal diagnostic means for explaining the different behaviour of both texture components during the anneal.

In the case of non-ordered b.c.c. metals and alloys various experimental methods were employed to investigate the elastically stored energy of grains with different orientations. Among these, X-ray line broadening experiments [43] and TEM investigations of the dislocation cell sizes of cold rolled specimens [44,45] seemed to provide the most reliable data. According to different authors [44,45] the cell sizes,  $C$ , change according to  $C_{\{001\}\langle 110 \rangle} < C_{\{112\}\langle 110 \rangle} < C_{\{111\}\langle uvw \rangle}$ . However, this information is rather coarse and does not – within the range of accuracy of the experimental techniques employed – allow for a distinction between {557}<110> and {111}<112> oriented crystals. Moreover, it is not certain whether these results are also valid for B2 and DO<sub>3</sub> ordered alloys.

In contrast to the vague arguments suggested above, a Taylor simulation of the slip systems involved during plastic deformation seems to provide a more plausible explanation for the behaviour observed. Allowing for 12 potential {110}<111> slip systems, {111}<112> oriented grains can be deformed by using only four different slip systems, even under FC Taylor conditions. In this case only two of these four active slip systems contribute 77% of the total amount of the required slip. Allowing for a further release of strain constraints (RC, pancake), only two of the three theoretically required

slip systems are necessary to achieve a solution. In the case that both 12  $\{110\}\langle 111\rangle$  and 12  $\{112\}\langle 111\rangle$  slip systems are considered in an FC model, plastic deformation of  $\{111\}\langle 112\rangle$  oriented grains is even attained by employing only three instead of four slip systems. In this case the two dominant glide systems contribute 80% of the total amount of slip. Using an RC pancake model even single slip conditions are predicted.

This slip analysis indicates that dislocation glide in  $\{111\}\langle 112\rangle$  oriented grains seems to be concentrated on a small number of slip systems. It is assumed that such a type of slip distribution gives only a moderate rise in the generation of large internal strains or local misorientations, which are both necessary prerequisites for primary recrystallization.

In case of  $\{557\}\langle 110\rangle$  oriented grains the corresponding simulations predict a more uniform distribution of slip. If dislocation glide is confined to  $\{110\}\langle 111\rangle$  systems in a FC model the two leading slip systems contribute only 62% to the total required shear. Due to the less symmetric position of the slip systems in the  $\{557\}\langle 110\rangle$  component, five instead of four systems must be activated under FC conditions and three instead of two systems under RC pancake conditions. If  $\{112\}\langle 111\rangle$  slip systems are additionally considered in an FC model only 65% of the total slip is contributed by the leading two of the five glide systems involved. Also, under RC pancake conditions the shear in  $\{557\}\langle 110\rangle$  is distributed more homogeneously on the slip systems involved than in  $\{111\}\langle 112\rangle$  oriented grains.

It is thus suggested that this more uniform activation of five (FC) or three (RC) slip systems gives rise to more complex dislocation reactions and thus to larger values of both stored energy and local misorientations when compared with  $\{111\}\langle 112\rangle$  oriented grains. On the basis of such an approach the recrystallization tendency of  $\{557\}\langle 110\rangle$  oriented crystals seems plausible.

The above analysis and the conclusions suggested essentially correspond to the results of the single orientation measurements (Figs. 5 and 6). However, whereas the texture changes observed via X-ray investigations supply statistical information, local texture determination enables one to consider the mechanisms involved in a more detailed manner.

As shown in Fig. 5, in numerous areas only small misorientations of less than  $20^\circ$  were observed between deformed and new grains. In such cases, where large recovered areas were observed, the Taylor factors of the deformation matrix were usually very low, which also suggests little strain hardening and thus little tendency to recrystallize. Grain B in Fig. 5 has an average Taylor factor of only 2.2 and grain F one of only 2.8. The same applies for the areas marked C and D in Fig. 5. The combination of a small average Taylor factor and

a weak tendency for recrystallization was confirmed for numerous deformed grains, which were inspected by use of EBSD. The observation that deformed and neighbouring newly formed grains were frequently related by a rotation about a common  $\langle 100\rangle$  axis (Fig. 7) underlines the assumption that recovery prevailed in deformed grains with a low Taylor factor. In a recent study Morris and Leboeuf [12] showed that during recovery of rolled  $\text{Fe}_3\text{Al}$  subgrain walls which consist of  $\langle 100\rangle$  Burgers vectors are indeed formed. In contrast, in deformed grains with orientations close to  $\{111\}\langle 110\rangle$  primary recrystallization, especially at former high angle grain boundaries, seemed to prevail. This can be seen in Fig. 6. The orientation of grain B is  $\sim\{557\}\langle 377\rangle$ , which is close to the main  $\{557\}\langle 110\rangle$  component shown in Fig. 3. The neighbouring deformed grain, C, has a  $\sim\{039\}\langle 862\rangle$  orientation which is close to  $\{001\}\langle 110\rangle$  on the  $\alpha$ -fibre. For grain B hence the same arguments apply which were already discussed as indicators for a large recrystallization tendency of  $\{557\}\langle 110\rangle$  oriented grains.

## 5. Conclusions

The texture and microstructure of a rolled and annealed  $\text{Fe}_3\text{Al}$  polycrystal was examined using optical and electron microscopy, single orientation determination and X-ray texture measurements. During rolling at  $560^\circ\text{C}$  a texture fibre close to  $\{111\}\langle uvw\rangle$  with a maximum at  $\{557\}\langle 110\rangle$  was generated. During annealing at  $750^\circ\text{C}$  the main features of the rolling texture were preserved. However, the  $\{557\}\langle 110\rangle$  orientation considerably decreased and the  $\{111\}\langle 112\rangle$  orientation stabilized. This observation was in accord with measurements carried out at the grain scale. The degradation of  $\{557\}\langle 110\rangle$  was attributed to recrystallization. The stabilization of  $\{112\}\langle 110\rangle$  was interpreted in terms of recovery. As indicated by the different behaviour of these two main texture components the study generally substantiated that neither recovery nor recrystallization homogeneously removed the deformation microstructure of  $\text{Fe}_3\text{Al}$  during annealing at  $750^\circ\text{C}$ . It was observed that both recovery and recrystallization took place preferably in deformed host grains with orientations which seemed to be characteristic of either of these two processes.

## Acknowledgements

The authors gratefully acknowledge the kind support by the University of Science and Technology, Beijing, China, especially by Professor Dr Z. Sun and Professor Dr W. Mao. The alloy used in this study was cast and thermomechanically hot rolled at the Department of

Materials Science and Engineering at the University of Science and Technology, Beijing. The authors are grateful to M. Büscher for carrying out the single orientation measurements.

## References

- [1] N. Ziegler, *Trans. AIME*, 100 (1932) 267.
- [2] W. Justusson, V.F. Zackay and E.R. Morgan, *Trans. Am. Soc. Metals*, 49 (1947) 905.
- [3] F. Lihl and R. Stickler, *Archiv Eisenhüttenwesen*, 31 (1960) 47.
- [4] A. Lawley, E.A. Vidoz and R.W. Cahn, *Acta Metall.*, 9 (1961) 287.
- [5] N.S. Stoloff and R.G. Davies, *Acta Metall.*, 12 (1964) 473.
- [6] H.J. Leamy, F.X. Kayser and M.J. Marcinkowski, *Phil. Mag.*, 20 (1969) 763, 779.
- [7] C.G. McKamey, J.H. De Van, P.F. Tortorelli and V.K. Sikka, *J. Mater. Res.*, 6 (1991) 1779.
- [8] C.G. McKamey, J.A. Horton and C.T. Liu, *J. Mater. Res.*, 4 (1989) 1156.
- [9] C.G. McKamey and C.T. Liu, *Scripta Metall.*, 24 (1990) 2119.
- [10] Z.Q. Sun, Y.D. Huang, W.Y. Yang and G.L. Chen, in I. Baker, R. Darloia, J.D. Whittenberger and M. Yoo (eds.), *High Temperature Ordered Intermetallic Alloys V*, Mater. Res. Symp. Proc., Pittsburgh, 1993, p. 885.
- [11] Z.Q. Sun, Y. Huang, W. Yang and G. Chen, *Proc. Conf. High Temperature Properties of Iron-based Aluminides*, TMS, San Francisco, in press.
- [12] D.G. Morris and M. Leboeuf, *Acta Metall.*, 42 (1994) 1817.
- [13] H.J. Leamy and F.X. Kayser, *Phys. Stat. Solidi*, 34 (1969) 765.
- [14] H.J. Leamy, E.D. Gibson and F.X. Kayser, *Acta Metall.*, 15 (1967) 1827.
- [15] L. Guttman, H.C. Schnyders and G.J. Arai, *Phys. Rev. Lett.*, 22 (1969) 520.
- [16] G. Lütjering and H. Warlimont, *Acta Metall.*, 12 (1964) 1460.
- [17] M.J. Marcinkowski and H.J. Leamy, *Phys. Stat. Solidi*, 24 (1967) 149.
- [18] H.J. Leamy, *Acta Metall.*, 15 (1967) 1839.
- [19] M.J. Marcinkowski and N. Brown, *Acta Metall.*, 9 (1961) 764.
- [20] M.J. Marcinkowski and N. Brown, *J. Appl. Phys.*, 33 (1962) 537.
- [21] T. Taoka and S. Sakata, *Acta Metall.*, 5 (1957) 19.
- [22] T. Taoka and R.J. Honda, *Electron Microsc. (Tokyo)*, 5 (1957) 19.
- [23] M.J. Marcinkowski, in *Electron Microscopy and Strength of Crystals*, Interscience, New York, 1963, p. 333.
- [24] W.A. Rachinger and A.H. Cottrell, *Acta Metall.*, 4 (1956) 109.
- [25] S. Takeuchi, in P. Haasen, V. Gerold and G. Kostorz (eds.), *Proc. 5th Int. Conf. Strength of Metals and Alloys*, Aachen, 1979, p. 53.
- [26] I. Baker and D.I. Gaydosh, *Mater. Sci. Eng.*, 96 (1987) 147.
- [27] Y. Umakoshi, in R.W. Cahn, P. Haasen and E.J. Kramer (eds.), *Materials Science and Technology*, Vol. 6, VCH, 1993, p. 251.
- [28] D.G. Morris, M.M. Dadras and M.A. Morris, *Acta Metall.*, 41 (1993) 97.
- [29] D. Raabe and K. Lücke, *Proc. 10th Int. Conf. Texture of Materials (ICOTOM 10)*, Materials Science Forum, 1994, 157–162, p. 597.
- [30] D. Raabe, K. Lücke, *Scripta Metall.*, 27 (1992) 1533.
- [31] D. Raabe, G. Schlenkert, H. Weisshaupt, K. Lücke, *Mater. Sci. Technol.*, 10 (1994) 229.
- [32] W. Mao and Z. Sun, *Scripta Metall.*, 29 (1993) 217.
- [33] W. Mao and Z. Sun, *Proc. 10th Int. Conf. Texture of Materials (ICOTOM 10)*, Materials Science Forum, 1994, 157–162, p. 1009.
- [34] D. Raabe, *Mater. Lett.*, 19 (1994) 75.
- [35] D. Raabe and W. Mao, *Phil. Mag. A*, 71 (1995) 805.
- [36] D. Raabe, *Comp. Mater. Sci.*, 3 (1994) 231.
- [37] M. Dahms and H.J. Bunge, *J. Appl. Cryst.*, 22 (1989) 439.
- [38] M. Dahms, *Text. Microstr.*, 19 (1992) 169.
- [39] J. Venables and C. Harland, *Phil. Mag.*, 27 (1973) 1193.
- [40] O. Engler and G. Gottstein, *Steel Res.*, 63 (1992) 413.
- [41] G.I. Taylor, *J. Inst. Met.*, 62 (1938) 307.
- [42] H. Honneff and H. Mecking, in G. Gottstein and K. Lücke (eds.), *Proc. 5th Int. Conf. Texture of Materials (ICOTOM 5)*, Vol. 1, Springer, 1978, p. 265.
- [43] J.L. Lebrun, G. Maeder and P. Parniere, in G. Gottstein and K. Lücke (eds.), *Proc. 5th Int. Conf. Texture of Materials (ICOTOM 5)*, Vol. 2, Springer, 1978, p. 513.
- [44] I.L. Dillamore, C.J.E. Smith and T.W. Watson, *Met. Sci. J.*, 1 (1967) 49.
- [45] D.J. Willis and M. Hatherly, in G. Gottstein and K. Lücke (eds.), *Proc. 5th Int. Conf. Texture of Materials (ICOTOM 5)*, Vol. 1, Springer, 1978, p. 465.